Available online at www.sciencedirect.com
ScienceDirect
Journal of Solid State Chemistry 179 (2006) 3347–3356
JOURNAL OF SOLID STATE CHEMISTRY
www.elsevier.com/locate/jssc

Oxygen permeability, thermal expansion and mixed conductivity of $Gd_xCe_{0.8-x}Pr_{0.2}O_{2-\delta}$, $x = 0$, 0.15, 0.2

D.P. Fagg*, I.P. Marozau, A.L. Shaula, V.V. Kharton, J.R. Frade

Department of Ceramics and Glass Engineering, CICECO, University of Aveiro, 3810-193 Aveiro, Portugal

Received 13 April 2006; received in revised form 23 June 2006; accepted 27 June 2006
Available online 29 June 2006

Abstract

The non-linear thermal expansion behaviour observed in $Ce_{1-y}Pr_yO_{2-\delta}$ materials can be substantially controlled by Gd substitution. Coulometric titration shows that the charge compensation mechanism changes with increasing x, in the system $Gd_xCe_{0.8-x}Pr_{0.2}O_{2-\delta}$. For $x = 0.15$, charge compensation is by vacancy formation and destabilises the presence of Pr^{4+}. At $x = 0.2$, further Gd substitution is charge compensated by additionally raising the oxidation state of Pr rather than solely the creation of further oxygen ion vacancies. Oxygen concentration cell e.m.f. measurements in an oxygen/air potential gradient show that increasing Gd content decreases ionic and electronic conductivities. Ion transference numbers measured under these conditions show a positive temperature dependence, with typical values $t_o = 0.90, 0.98$ and 0.80 for $x = 0, 0.15$ and 0.2, respectively, at 950 °C. These observations are discussed in terms of defect association. Oxygen permeation fluxes are limited by both bulk ambipolar conductivity and surface exchange. However, the composition dependent trends in permeability are shown to be dominated by ambipolar conductivities, and limited by the level of electronic conductivity. At the highest temperatures, oxygen permeability of composition $x = 0.2$ approaches that of composition $x = 0$, $Ce_{0.8}Pr_{0.2}O_{2-\delta}$, with specific oxygen permeability values approximately 2×10^{-9} mol s^{-1} cm^{-1} at 950 °C, but offering much better thermal expansion properties.

Keywords: Praseodymium–cerium–gadolinium oxide; Transference number; Oxygen permeation; Thermal expansion; Ionic conductivity; Fluorite; Defect association

1. Introduction

The solid solution system $Ce_{1-y}Pr_yO_{2-\delta}$ can accommodate extensive deviations from stoichiometry with high rates of oxygen exchange and diffusion, whilst offering good stability in repeated redox cycles, features which are of great importance for possible uses such as gas sensors, catalyst supports and/or oxygen storage materials in automotive catalysis [1–7]. Furthermore, it has been suggested that these materials may be promising for oxygen separation membranes, with oxygen permeabilities rivalling that of mixed conductors based on the best conductive bismuth oxide solid electrolytes [8]. Shuk and Greenblatt [8] demonstrated that at Pr contents greater than 25 at%, the electronic conductivity of the system $Ce_{1-y}Pr_yO_{2-\delta}$ was shown to exceed that of the ionic conductivity at temperatures $\leqslant 700$ °C. As maximum oxygen fluxes are promoted in mixed conducting oxygen separation membranes which offer equally high electronic and ionic conductivities, the oxygen permeabilities exhibited by the system $Ce_{1-y}Pr_yO_{2-\delta}$ at 700 °C were suggested to show a maximum at $y = 0.3$, where ionic and electronic conductivities were equal, yielding a theoretical value of oxygen permeability $J(O_2) = 1.9 \times 10^{-10}$ mol s^{-1} cm^{-1} [8]. At higher temperatures, predominately ionic conductors can be obtained as the ion transference numbers of these materials show positive temperature dependences [8–10], for example the composition $Ce_{0.8}Pr_{0.2}O_{2-\delta}$ exhibits an ion transference number $t_o = 0.9$ at 950 °C [10]. As a consequence, although compositions in this system with values of y in the range $0.2 < y < 0.3$ may offer competitive levels of oxygen permeability at intermediate temperatures, at higher temperatures (>700 °C) the permeability becomes

*Corresponding author. Fax: +351 234 425300.
E-mail address: duncan@cv.ua.pt (D.P. Fagg).

0022-4596/$ - see front matter © 2006 Elsevier Inc. All rights reserved.
doi:10.1016/j.jssc.2006.06.028

limited by the low level of electronic conduction [9]. The level of electronic conductivity could be most simply increased by increasing the concentration of Pr. However, this is prevented in these materials due to the extent of the cubic defect fluorite solid solution, which is reported to exist only up to values of $x = 0.3$ [7,8,11,12]. Further enhancement of electronic conductivity in these materials therefore must come from the introduction of additional dopants.

The system $Ce_{1-y}Pr_yO_{2-\delta}$ suffers a high and non-linear thermal expansion behaviour which is exacerbated with increasing Pr content [9,11,12]. For example, the average thermal expansion coefficient (TEC) observed by dilatometry for the material $Ce_{0.8}$ $Pr_{0.2}O_{2-\delta}$ is reported to vary between 10 and $30 \times 10^{-6}\,K^{-1}$ across different temperature ranges between 0 and 1000 °C [11,12]. Such a fluctuation of TEC may limit possible practical uses due to mismatch with other components and associated failure. Steele et al. [11,12] recently tried to introduce Nb into $Ce_{1-y}Pr_yO_{2-\delta}$ materials. The introduction of 5 at% Nb into 8 at% Pr-containing CeO_2 radically modified thermal expansion behaviour, lowering and stabilising the TEC [12]. However, the presence of 5% Nb was not fully accommodated into the fluorite structure, producing a secondary monoclinic phase that lowered conductivity [12]. At higher Pr levels, the presence of 3% Nb was shown not to be able to control thermal expansion behaviour although single-phase materials were produced [11]. Alternatively, recent work by our group has shown that TEC can be controlled by substitution of 10 at% Zr for Ce [9], for example, substitution of 10 at% Zr for cerium forming the composition $Zr_{0.1}Ce_{0.7}$ $Pr_{0.2}O_{2-\delta}$ gives average TECs varying between 13 and $18 \times 10^{-6}\,K^{-1}$ across the temperature range 30–1000 °C. Unfortunately substitution of Zr also leads to the negative effect of a decreased total conductivity [9].

In this work, the influence of substitution of Gd for Ce is assessed. Here, the presence of Gd may be charge compensated by either an increase in oxygen vacancy concentration or by an increase in the average oxidation state of Pr. In previous results, the average oxidation state of Pr in $Ce_{1-y}Pr_yO_{2-\delta}$ in air was shown to vary between approximately 3.3+ to 3.2+ across the temperature range 800–950 °C [10]. Any increase in the average oxidation state of Pr due to charge compensation for further dopants may be beneficial in terms of enhancing p-type conductivity. Here we assess the influence of Gd substitution on resultant conductivity in oxidising conditions, separating partial conductivities by ion transference numbers obtained by oxygen concentration cell e.m.f. measurements. The coulombic titration technique is used to study the influence of Gd substitution on the result average Pr oxidation state and all of these results are united to assist in the explanation of variations in oxygen permeability. The impact of Gd substitution on thermal expansion behaviour is also assessed.

2. Experimental

2.1. Sample preparation, microstructural and phase analysis

Compositions $x = 0, 0.15$ and 0.2 in the system $Gd_xCe_{0.8-x}Pr_{0.2}O_{2-\delta}$ were prepared. Stoichiometric amounts of high-purity Pr_6O_{11}, $Gd(NO_3)_3 \cdot 6H_2O$ and $Ce(NO_3)_3 \cdot 6H_2O$ were dissolved an aqueous solution of hot nitric acid. After drying, the nitrate mixture was decomposed at 700 °C. The resultant powder was ball-milled in a nylon mill with zirconia balls. The milled powder was dry pressed into pellets (diameter of 20 mm, pressure of 30 MPa) followed by isostatic pressing at 200 MPa. These pellets were then sintered at 1600 °C for 10 h followed by cooling at $2\,°C\,min^{-1}$. Overall phase composition was determined by X-ray diffraction (XRD) using a Rigaku Geigerflex diffractometer (CuK_α radiation), (5–80°, step 0.02, $0.4\,s\,step^{-1}$); unit cell parameters were determined using Materials Data Inc. Jade6 software, pseudo Voight profile fit and an external silicon standard for zero point correction. Microstructural characterisation was performed by scanning electron microscopy (SEM), Hitachi H9000-NA, on ceramic samples, polished and then thermally etched for 60 min at temperature 100 K below that of the sintering temperature. Data on oxygen stoichiometry was obtained by thermogravimetric analysis (TGA), Setaram Labsys 1600.Rod, in the cooling mode. Samples were heated to 1000 °C and held at this temperature for 1 h, followed by cooling at $2\,°C\,min^{-1}$ to room temperature, during which oxygen uptake was monitored. Variations in oxygen content were measured as a function of oxygen partial pressure and temperature with respect to a reference point of air by means of the coulometric titration technique in the double electrochemical cell in potentiostatic mode, as described elsewhere [13].

2.2. Electrical characterisation and oxygen permeability

Total conductivity in air was performed in the 4-electrode configuration on dense bars, approximately $2 \times 4 \times 8$ mm using the a.c. impedance method. Steady-state oxygen permeability was performed as described elsewhere [14,15]. All data on the oxygen permeability presented in this paper correspond to the membrane feed-side oxygen partial pressure ($p2$) equal to 0.21 atm, atmospheric air. The permeation processes are discussed using the quantities of oxygen flux density, j, and specific oxygen permeability, $J(O_2)$, which are interrelated as

$$J(O_2) = jd\left[\ln\frac{p2}{p1}\right]^{-1}, \quad (1)$$

where $p1$ is the oxygen partial pressure at the membrane permeate side ($p1 < p2$). The thickness of the ceramic membranes (d) varied from 1.0 to 1.4 mm. The quantity

$J(O_2)$ is useful to identify surface exchange rate-limiting effects on oxygen permeation by analysing the dependence of the permeation flux on membrane thickness.[14,15]. As this quantity is proportional to *jxd by definition*, the values of $J(O_2)$ should be thickness independent when surface limitations are negligible. In this situation, $J(O_2)$ is proportional to the ambipolar conductivity (σ_{amb}), averaged for a given oxygen partial pressure range ($\overline{\sigma_{amb}}$) where t_o is the oxygen ion transference number, and σ, σ_o and σ_e represent the total, oxygen ionic, and electronic conductivities, respectively:

$$J(O_2) = \frac{RT}{16F^2}\overline{\sigma_{amb}} = \frac{RT}{16F^2}\frac{\overline{\sigma_o\sigma_e}}{\sigma_o + \sigma_e} = \frac{RT}{16F^2}\overline{\sigma t_o(1 - t_o)}. \quad (2)$$

When oxygen surface exchange limitations are considerable, the values of $J(O_2)$ should increase with membrane thickness due to a decreasing role of the surface exchange, for a given oxygen chemical potential gradient.

Minor electron-hole conductivity was separated from total electrical conductivity using the modified e.m.f. method first proposed by Gorelov [16]. This modification of the classical e.m.f. technique, based on determination of the open-circuit voltage of oxygen concentration cells, increases measurement sensitivity and eliminates possible errors in the determination of ion transference numbers arising due to electrode polarisation, errors that are shown to be non-negligible for electrolyte-type materials which possess relatively minor electronic conductivity [17,18]. The experimental set-up, measurement procedure and also comparison of this technique with the traditional approach are well documented in the literature [17,18].

3. Results and discussion

3.1. Structure and ceramic microstructure

The relative density of materials synthesised from their component metal nitrates is shown to be greater than 90% that of the theoretical density, with no open porosity, Table 1. All compositions exhibit the cubic defect fluorite structure. No evidence of secondary phases was discernable by XRD. Calculated lattice parameters for the Gd-containing compositions are shown in Table 1 and compared to the value for the composition $Ce_{0.8}Pr_{0.2}O_{2-\delta}$ taken from reference [9]. No simple trend between lattice parameter and composition is observed as lattice parameter is highly dependent on the oxidation state of Pr, as documented in the literature [4,9]. The microstructures of all compositions studied are similar with no significant variation in grain size (Fig. 1). Fig. 1 also shows that good-quality ceramics can be made by this synthesis route. Average grain size is between 3 and 6 μm.

Table 1
Lattice parameter and relative density of $Gd_xCe_{0.8-x}Pr_{0.2}O_{2-\delta}$ ceramics as prepared in air

Composition x	Relative density (%)	Lattice parameter (nm) (± 0.0004 nm)
0	92.7	0.5437
0.15	95.2	0.5442
0.2	93.2	0.5440

3.2. Thermal expansion and variations in oxygen stoichiometry in air

The thermal expansion results reported in Fig. 2a and b demonstrate that the highly non-linear thermal expansion behaviour exhibited by the composition $Ce_{0.8}Pr_{0.2}O_{2-\delta}$ ($x = 0$) can be successfully controlled by Gd substitution in the system $Gd_xCe_{0.8-x}Pr_{0.2}O_{2-\delta}$, $x = 0.15, 0.2$. Plotting the differential of the thermal expansion plot, Fig. 2b, helps to clarify that a large increase in thermal expansion rate occurs at intermediate temperatures around 600 °C. As the value of x increases, this large increase in thermal expansion rate is diminished, yielding values of TEC which vary between 10 and $18 \times 10^{-6}\,K^{-1}$ across different temperature ranges between 0 and 1000 °C, for the composition $x = 0.2$. In the related system $Ce_{1-x}Gd_xO_{2-\delta}$, it has been noted that Gd substitution (up to $x = 0.2$) increases TEC and this was suggested to be due to a weakened metal–oxygen (M–O) binding energy [19]. Hence, the inverse trend of regulation of TEC by increased Gd content in the $Gd_xCe_{0.8-x}Pr_{0.2}O_{2-\delta}$ system is interesting as it cannot be explained from a similar discussion of average M–O bond strength.

In a previous publication, the large increase in thermal expansion at intermediate temperatures in the system $Ce_{1-y}Pr_yO_{2-\delta}$ was shown to be related to rapid changes in oxygen stoichiometry, which could be controlled by Zr substitution [9]. The temperature variation of oxygen stoichiometry in air, assessed by thermogravimetry, for the current system $Gd_xCe_{0.8-x}Pr_{0.2}O_{2-\delta}$ is shown in Fig. 3. The uptake of oxygen on cooling is less for higher values of x, suggesting less facile redox behaviour as the concentration of Gd increases. This observation again conflicts with literature data for the related system $Gd_xCe_{1-x}O_{2-\delta}$. Experimentally, more facile redox behaviour is reported in the system $Gd_xCe_{1-x}O_{2-\delta}$ for increased Gd contents (up to $x = 0.2$) [20–22], a phenomenon recently modelled by atomistic simulations [23]. Nevertheless, the depleted levels of atmospheric oxygen exchange for compositions containing gadolinium reported in Fig. 3 reinforce the results of Fig. 2a and b, which show control of thermal expansion behaviour by increased gadolinium substitution in the current system. Hence, to further understand the redox behaviour in the system $Gd_xCe_{0.8-x}Pr_{0.2}O_{2-\delta}$, the oxygen partial pressure dependence of oxygen non-stoichiometry is studied by the coulombic titration technique.

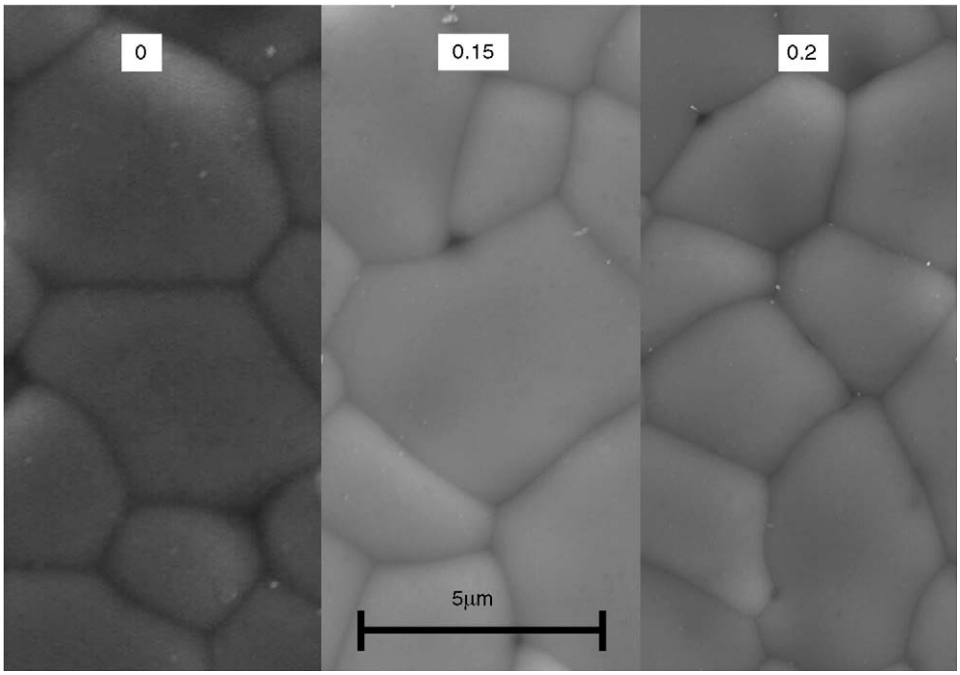

Fig. 1. SEM micrographs for the system $Gd_xCe_{0.8-x}Pr_{0.2}O_{2-\delta}$, $x = 0, 0.15$ and 0.2. The values of x are indicated on the figure.

3.3. Oxygen non-stoichiometry

The coulometric titration results for compositions $Gd_xCe_{0.8-x}Pr_{0.2}O_{2-\delta}$, where $x = 0, 0.15$ and 0.2 are presented in Fig. 4a and b in the form of $pO2$–T–$\Delta\delta$ diagrams for the oxygen partial pressure range 10^{-4}–0.21 atm with respect to a reference point of air. As oxygen partial pressure decreases, oxygen non-stoichiometry increases and the magnitude of this increase exhibits negative temperature dependence. At each temperature, the magnitude of the change in oxygen non-stoichiometry with pO_2 is least for composition $x = 0.15$, while the compositions $x =$ 0 and 0.2 show similar values.

The non-stoichiometries of similar ceria-based defect fluorite materials, for example, pure $CeO_{2-\delta}$ or doped cerias such as Sm-, Gd- or Y-ceria, are comprehensively documented in the literature. Gravimetric studies by authors such as Wang et al. [21] or Bevan and Kordis [24] demonstrate clearly that for either pure ceria or Gd-doped ceria materials, significant reduction of Ce^{4+} initiates at oxygen partial pressures lower than 10^{-10} atm, whereas at higher pO_2 values, oxygen non-stoichiometry is observed to be effectively constant. In comparison, the materials of the present study contain two cations, Pr and Ce, which have the capacity to exhibit mixed valency. In Fig. 4a and b, oxygen non-stoichiometry can be seen to substantially increase immediately as pO_2 decreases from air. It is therefore reasonable to suggest that the changes in oxygen non-stoichiometry observed at the much more oxidising conditions ($<10^{-5}$ atm) in the current experiment are more likely related to the reduction of Pr^{4+} rather than severe destabilisation of Ce^{4+}. Recent work demonstrated that this assumption allowed the pO_2 dependence of conductivity of the system $Ce(Pr,Zr)O_{2-\delta}$ to be effectively categorised from the defect chemistry [10]. In a similar way, the dominant defect equilibrium at higher oxygen partial pressures in the system $Gd_xCe_{0.8-x}Pr_{0.2}O_{2-\delta}$ is thereby suggested to be that of Pr reduction which is given by the equation

$$2Pr^x_{Ce} + O^x_O \overset{K}{\longleftrightarrow} 2Pr'_{Ce} + V^{\bullet\bullet}_O + \frac{1}{2}O_2, \tag{3}$$

where the Kröger Vink notation is used leading to the relationship describing equilibrium constant for Pr reduction,

$$K = \frac{[V^{\bullet\bullet}_O][Pr'_{Ce}]^2 pO_2^{1/2}}{[Pr^x_{Ce}]^2[O^x_O]}. \tag{4}$$

Following the typical Brouwer approach [25], the electroneutrality relation under these higher oxygen partial pressures can be simplified as

$$[Pr'_{Ce}] + [Gd'_{Ce}] = 2[V^{\bullet\bullet}_O]. \tag{5}$$

as both $[Pr'_{Ce}]$ and $[Gd'_{Ce}] \gg [Ce'_{Ce}]$ at high pO_2.

For any composition given by the general formula $Gd_xCe_{0.8-x}Pr_{0.2}O_{2-\delta}$, one can write the overall reduction reaction as

$$Ce_{0.8-x}Pr_{0.2}Gd_xO_{2-\delta} \leftrightarrow Ce_{0.8-x}Pr_{0.2}Gd_xO_{2-x/2-\alpha} + \frac{\alpha}{2}O_2 \tag{6}$$

and using the electroneutrality relation Eq. (5),

$$[O^x_O] = 2 - x/2 - \alpha, \tag{7}$$

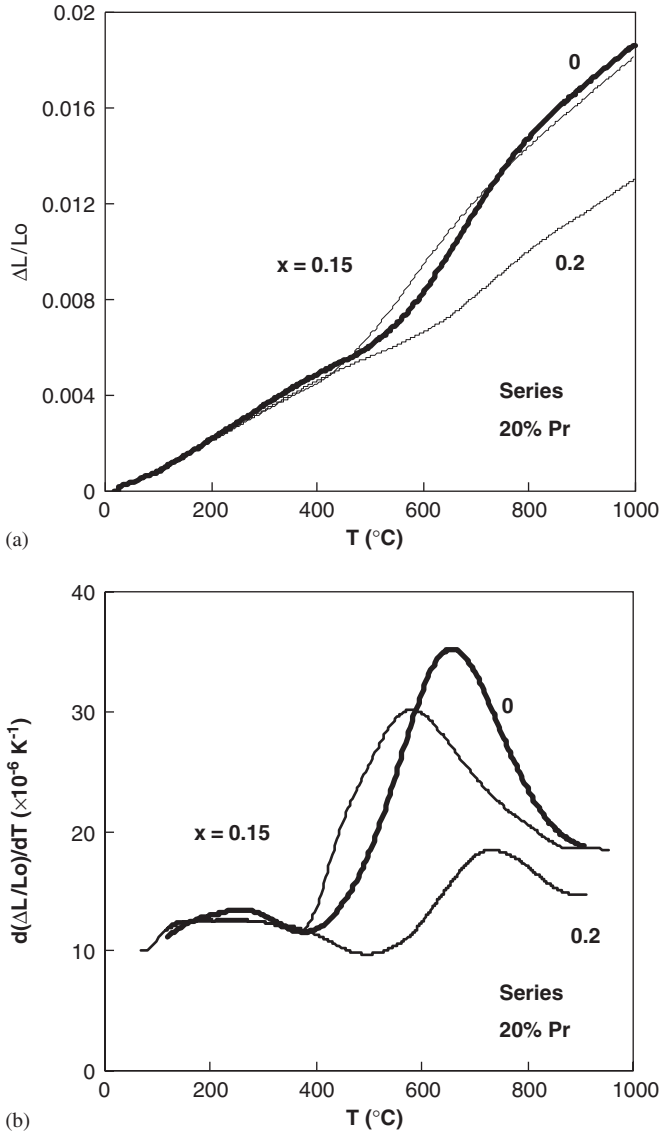

Fig. 2. (a) Thermal expansion behaviour in the system $Gd_xCe_{0.8-x}Pr_{0.2}O_{2-\delta}$, for $x = 0, 0.15$ and 0.2, and (b) the differential of the thermal expansion plot clarifying the observation that the large increase in thermal expansion rate at intermediate temperatures is diminished with increasing x.

$$[V_O^{\cdot\cdot}] = x/2 + \alpha, \tag{8}$$

$$[Pr_{Ce}^{x}] = 0.2 - 2\alpha, \tag{9}$$

$$[Pr_{Ce}^{\prime}] = 2\alpha. \tag{10}$$

Clearly, one can rewrite Eq. (4) to describe the pO_2 dependence of the change in oxygen non-stoichiometry due to the reduction of Pr, α, using Eqs. (5)–(10):

$$K = \frac{4\alpha^2(x/2+\alpha)pO_2^{1/2}}{(0.2-2\alpha)^2(2-x/2-\alpha)}. \tag{11}$$

Values of K can subsequently be determined which best describe the experimental dependence of sample oxygen non-stoichiometry on pO_2 for each value of x, as presented

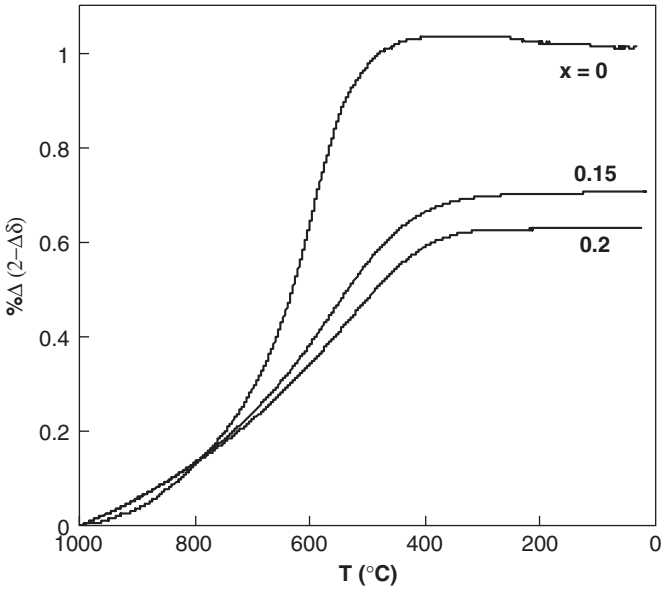

Fig. 3. Temperature dependence of the percentage change in oxygen stoichiometry on cooling from 1000 °C for the system $Gd_xCe_{0.8-x}Pr_{0.2}O_{2-\delta}$, $x = 0, 0.15$ and 0.2.

in Fig. 4a and b, constrained by relationship, Eq. (11). In Fig. 4a and b, $\Delta\delta = [V_O^{\cdot\cdot}] - [V_O^{\bullet\bullet}]^{air} = \Delta\alpha$, where $\Delta\alpha$ represents the change in oxygen non-stoichiometry resulting from the reduction of Pr from a reference point of air. The best-fit values of K are summarised in Table 2 whilst the solid lines in Fig. 4a and b describe the fit to the experimental data. The fractional concentration of Pr in the 3+ oxidation state can be calculated as

$$\frac{[Pr_{Ce}^{\prime}]}{[Pr_{Ce}]_{Total}} = \frac{2\alpha}{0.2}. \tag{12}$$

Fig. 5 represents the pO_2 dependence of the fractional concentration of Pr in the 3+ oxidation state calculated for the values of equilibrium constant K given in Table 2. At elevated temperatures, the average oxidation state of praseodymium in these Gd-containing materials in air is calculated to be very low for all compositions and lowest for composition $x = 0.15$. Furthermore, the composition containing most gadolinium, $x = 0.2$, shows a similar fractional concentration of Pr^{3+} to composition $Ce_{0.8}Pr_{0.2}O_{2-\delta}$, ($x = 0$). For all compositions, the calculations predict that all Pr is reduced by approximately 10^{-8} atm.

The increase in Gd content from $x = 0$ to 0.15 is, therefore, accommodated by vacancy formation and destabilises the presence of Pr^{4+}. What is interesting is that this trend is not continued in $Gd_xCe_{0.8-x}Pr_{0.2}O_{2-\delta}$ for the composition $x = 0.2$. In the case of $x = 0.2$, the further Gd substitution is instead charge compensated by additionally raising the oxidation state of Pr rather than solely the creation of additional oxygen ion vacancies, (Fig. 5). The enthalpy of reduction $\Delta\overline{H_O}$ can be calculated by

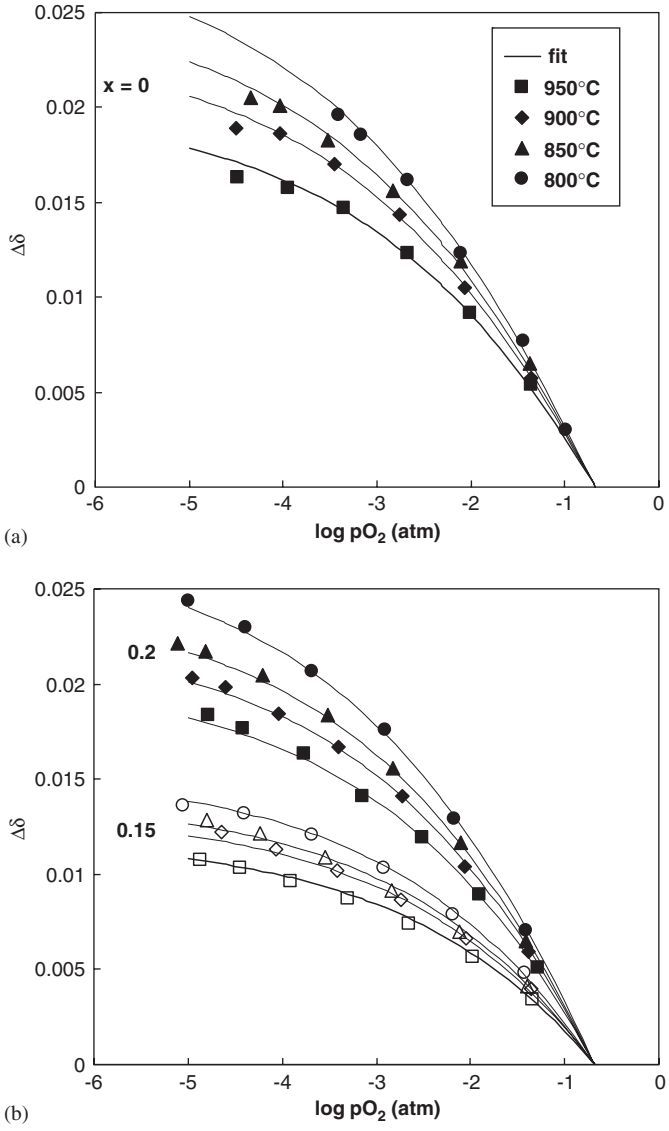

Fig. 4. Oxygen partial pressure dependence of oxygen non-stoichiometry with respect to a reference point of air in the system $Gd_xCe_{0.8-x}Pr_{0.2}O_{2-\delta}$ for (a) the composition $x = 0$ and (b) the compositions $x = 0.15$ and 0.2. The values of x are indicated on the figure.

Table 2
Best-fit values of equilibrium constant K for Pr reduction (Eq. (1)).

T (°C)	Composition		
	0	0.15	0.2
	$K \pm 0.005$	$K \pm 0.01$	$K \pm 0.005$
950	0.300	2.20	0.690
900	0.196	1.70	0.520
850	0.150	1.50	0.420
800	0.107	1.20	0.310

re-plotting the fitted data in Fig. 5 in the form $\ln pO_2$ versus $1/T$ for various values of α, and extracting the gradient. [21]. The values of $\Delta\overline{H_O}$ are calculated to be -73 ± 6, -42 ± 4 and $-57 \pm 3\,kJ\,mol^{-1}$ for compositions $x = 0$, 0.15 and 0.2, respectively, obtained from data above 800 °C. These values support the lower Pr oxidation state exhibited by composition $x = 0.15$, in Fig. 5. The values also correspond well with literature values for the reduction of $PrO_{2-\delta}$ [26] supporting the assumption that dominant defect equilibrium at higher oxygen partial pressures is that of the reduction of Pr (Eq. (3)) (typical $\Delta\overline{H_O}$ values for Ce reduction are approx. around $-400\,kJ\,mol^{-1}$ [21,27]). A maximum in the enthalpy of reduction has been noted both in the system $CeO_{2-\delta}$, at values of $\delta > 0{\cdot}15$, and in the system $Ce_{1-x}Gd_xO_{2-\delta}$ for values of $x > 0.3$ (i.e., also at values of $\delta > 0.15$) [27,28]. Typically, the existence of such maxima is attributed to ordering phenomena. As δ increases beyond the maximum (either due to reduction or further aliovalent doping), $\Delta\overline{H_O}$ becomes more negative and further reduction energetically unfavourable due to the necessity of ordering. The oxygen non-stoichiometry δ in air in the current system $Gd_xCe_{0.8-x}Pr_{0.2}O_{2-\delta}$, for $x = 0.15$ and $x = 0.2$, is predicted by Fig. 5 to be in this elevated range, i.e., $\delta > 0.15$. A similar hypothesis in the present system, therefore, can be suggested, that at high values of x the charge compensation mechanism changes as the introduction of further vacancies becomes energetically unfavourable due to ordering. Moreover, vacancy associates have been suggested to be of the form $(M'_{Ce}V_O^{\bullet\bullet}M'_{Ce})^x$ [29], where in the present case M'_{Ce} could be either Gd^{3+} or Pr^{3+}. The involvement of Pr^{3+} in vacancy clusters may lead to its stabilisation, for example, as possibly seen in Fig. 5 for composition $x = 0.15$. At higher Gd contents, the charge compensation mechanism is observed to change, leading to an increase in Gd'_{Ce} concentration without further major increases in oxygen vacancy concentration. One can envisage that, due to the increased statistical concentration, more vacancy associates would now involve

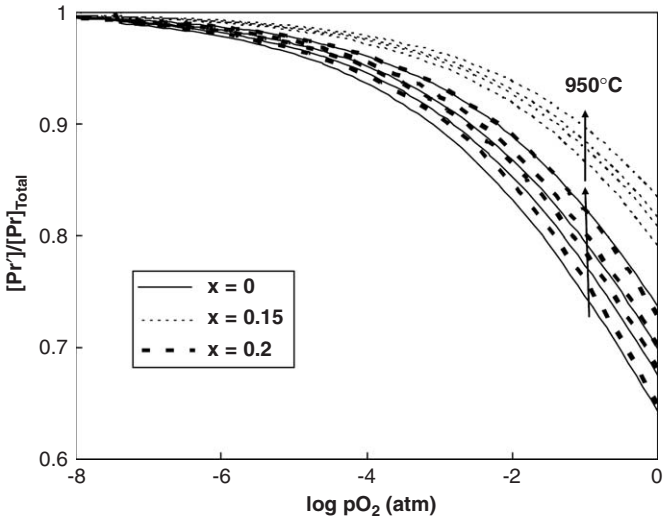

Fig. 5. Calculated oxygen partial pressure dependence of the fractional concentration of Pr in the 3+ oxidation state in the system $Gd_xCe_{0.8-x}Pr_{0.2}O_{2-\delta}$ for $x = 0$, 0.15 and 0.2 at 800, 850, 900, 950 °C. Arrows indicate direction of increasing temperature.

Gd^{3+}. The number of Pr ions not involved in vacancy associates would be increased, allowing charge compensation by an increase in the average oxidation state of Pr.

Furthermore, the temperature dependence of thermal expansion (Fig. 2a and b) and variation of oxygen stoichiometry in air (Fig. 3) possibly can also be explained from consideration of ordering phenomena. This is due to the requirement of a vacancy disassociation enthalpy before oxygen ions can be exchanged with the atmosphere. Vacancy association is typical of defect fluorite oxide materials and the temperature at which these vacancy associates dissociate is shown to be composition dependent [30,31]. The values of $\Delta\overline{H_O}$ calculated from Fig. 5 are from analysis of data above 800 °C, at lower temperatures vacancies can be considered fully clustered and the enthalpy of reduction may well involve an additional enthalpy of vacancy disassociation. In addition, the enthalpy of vacancy disassociation would be dependent on cluster composition, a factor linked to the level of Gd substitution. It is suggested, therefore, that an increase in the vacancy disassociation enthalpy with increasing x would lead to lower oxygen exchange with the atmosphere with temperature, an effect most notable at lower temperatures when the energy required for vacancy disassociation is not available. At the largest Gd substitutions, these vacancy associates may indeed persist to elevated temperatures.

3.4. Ionic, electronic and total conductivity

The temperature dependence of total conductivity in air is shown in Fig. 6a for compositions $Gd_xCe_{0.8-x}Pr_{0.2}O_{2-\delta}$, $x = 0, 0.15$ and 0.2. The apparent activation energy for total conduction of composition $x = 0$ is not constant with temperature, Table 3. Inflexion occurs at approximately 600–700 °C, which corresponds well with dilatometric and thermogravimetric results which described large changes in oxygen stoichiometry for this composition in this temperature range, Fig. 2a and b and Fig. 3 respectively. Moreover, the lower oxygen exchange with temperature noted for Gd-containing compositions may explain the more linear total conductivity slopes for these materials. A higher total conduction is observed for composition $x = 0$, while $x = 0.15$ and $x = 0.2$ are similar.

The modified e.m.f. technique takes the electrode polarisation into account and, thus, enables precise separation of the partial ionic and electronic contribution to the total conductivity [16–18]. Fig. 6b presents the

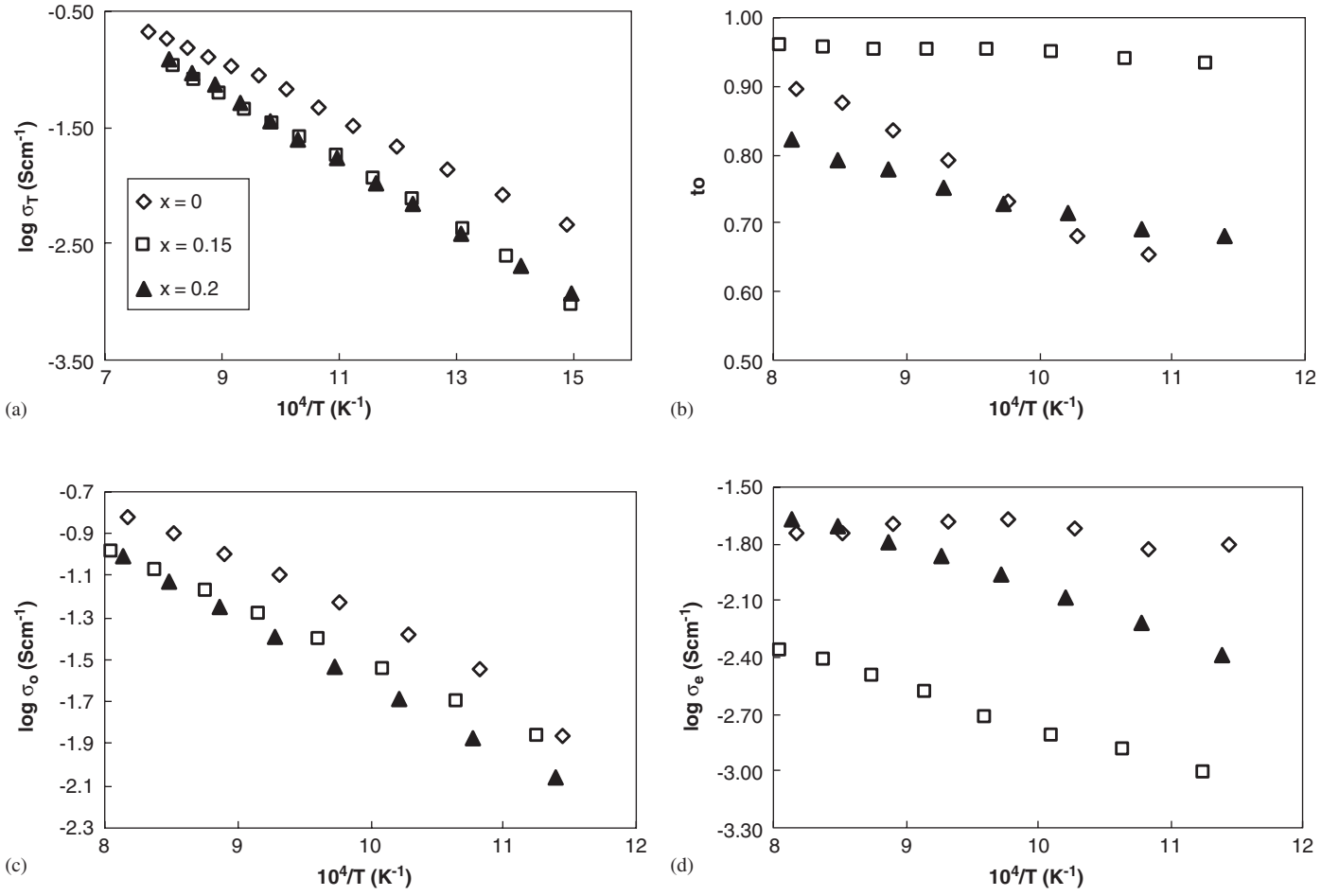

Fig. 6. Temperature dependence of (a) total conductivity, (b) ionic transference number, (c) ionic conductivity, (d) electronic conductivity in the system $Gd_xCe_{0.8-x}Pr_{0.2}O_{2-\delta}$ for $x = 0, 0.15$ and 0.2, in the oxygen partial pressure gradient, 1/0.21 atm.

Table 3
Apparent activation energies (E_a) for the total conductivity (σ_T) measured in air and the partial ionic conductivity (σ_o) measured in an oxygen/air pO_2 gradient for $Gd_xCe_{0.8-x}Pr_{0.2}O_{2-\delta}$ ceramics

Composition x	σ_T		σ_o	
	E_a (kJ mol^{-1})	Temperature range (°C)	E_a (kJ mol^{-1})	Temperature range (°C)
0	53.1±2	400–700	65.8±1	650–800
	48.6±1	700–1000	56.9±2	800–950
0.15	59.2±2	450–950	61.0±1	600–950
0.2	64.8±2	450–950	70.5±1	600–950

oxygen ion transference numbers (t_o) obtained for the compositions $x = 0, 0.15$ and 0.2 by the e.m.f. method, averaged across the $p(O_2)$ gradient 1/0.21 atm (oxygen/air). Combining transference numbers with the total conductivity (σ_T) values obtained by impedance spectroscopy at corresponding temperatures allows ionic conductivities (Fig. 6c) to be estimated as

$$\sigma_o = t_o\sigma_T. \tag{13}$$

The activation energy (E_a) for the partial ionic conductivities is calculated by the standard Arrhenius equation:

$$\sigma_o = \frac{A_0}{T}\exp\left[-\frac{E_a}{RT}\right], \tag{14}$$

where A_o is the pre-exponential factor, Table 3.

The ionic transference number decreases with decreasing temperature, in agreement with previous work on the related systems $Ce_{1-y}Pr_yO_{2-\delta}$ [8–10] and $Zr_{0.1}Ce_{0.7}Pr_{0.2}O_{2-\delta}$ [9,10] under similar oxygen potential gradients. Fig. 6b shows that these materials are predominantly ionic conductors at elevated temperatures, under these oxidising conditions. The ionic transference number is highest for composition $x = 0.15$ and shows the weakest temperature dependence. The strongest temperature dependence is exhibited by $x = 0$, causing the ionic transference number to deplete to values below that observed for $x = 0.2$ at lower temperatures. The ionic conductivity is shown to decrease with increasing aliovalent substitution, an observation typical of defect fluorite materials at high levels of oxygen non-stoichiometry, in the so-called "concentrated regime" [30] (Fig. 6c). The activation energy for ionic conduction shows temperature dependence for composition $x = 0$, while for the other compositions, it is effectively temperature independent within the studied temperature range, Table 3. This can be related to the large temperature dependence of oxygen stoichiometry noted in Fig. 3 for composition $x = 0$. If we compare the activation energies for ionic conductivity for $x = 0.15$ and $x = 0.2$ to that of $x = 0$ at high temperatures 800–1000 °C, we observe a substantial increase in activation energy when $x = 0.2$, Table 3. This observation supports the discussion in Section 3.2 which suggested that vacancy associates may persist to elevated temperatures especially for higher values of x.

The electronic conductivities (Fig. 6d) are estimated as

$$\sigma_e = (1 - t_o)\sigma_T. \tag{15}$$

The electronic conductivity in these materials has been stated in a previous publication to arise due to small polaronic hopping between adjacent Pr ions and to be proportional to the product of the concentration of charge carriers and the concentration of available sites to which small polaronic electron hops can progress [10]. In Fig. 6d, the electronic conductivities of $x = 0$ and $x = 0.2$ are similar at the highest temperatures, as perhaps could be expected from their similar fractional concentrations of Pr^{3+} at these temperatures, as shown in Fig. 5. The electronic conductivity of $x = 0.15$ is much smaller and reflects the higher fractional concentration of Pr^{3+} in this composition and related decrease in the number of mobile electronic charge carriers as the product of the concentration of charge carriers and the concentration of available sites decreases [10] (Fig. 5). Interestingly, the electronic conductivity has positive temperature dependence in the compositions $x = 0.15$ and $x = 0.2$ (Fig. 6d), despite a decrease in the number of mobile electronic charge carriers with increasing temperature (Fig. 5). This is due to larger activation energy for small polaronic conduction in compositions containing Gd, probably related to vacancy-acceptor ordering phenomena, which make electron transfer between Pr^{3+} and Pr^{4+} energetically unfavourable.

3.5. Oxygen permeability

Fig. 7 shows the steady-state oxygen permeation flux (A) and the corresponding specific oxygen permeability (B) through membranes of $x = 0, 0.15$ and 0.2 as a function of oxygen chemical potential gradient. The variation between the specific oxygen permeability, $J(O_2)$, values of membranes of different thickness is shown for the composition $x = 0.15$ to be significant and outside the limits of experimental error, suggesting that these materials are limited by both bulk ambipolar conductivity and surface exchange. For such a case, the integral form of the Wagner equation is not obeyed and the ion transference numbers cannot be extracted from the oxygen permeation flux. Fig. 8 compares the oxygen permeation flux for compositions $x = 0, 0.15$ and 0.2 for identical membrane thicknesses and oxygen potential gradients. The general trends of variation in permeation flux with composition have a strong base in the ambipolar conductivities of these materials. This can be explained with reference to Fig. 9, which plots the ambipolar conductivities of these materials calculated from the results of e.m.f. measurements (Fig. 6a–d) and Ref. [10] as

$$\sigma_{amb} = \frac{\sigma_e\sigma_o}{\sigma_e + \sigma_o}. \tag{16}$$

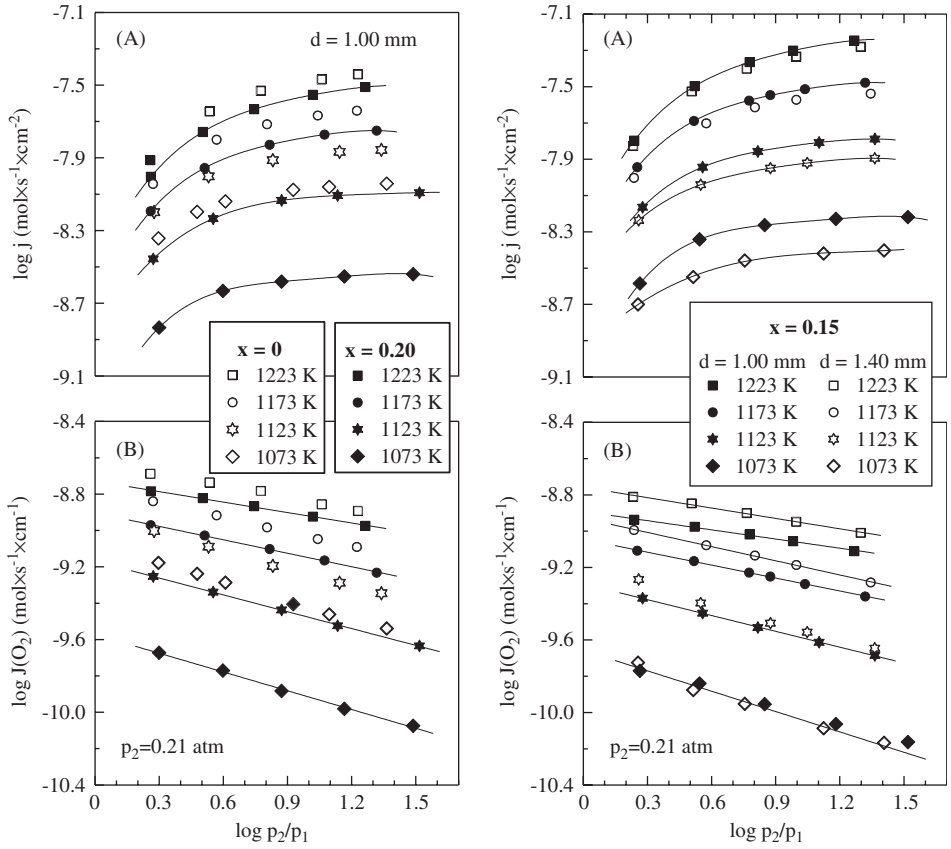

Fig. 7. Oxygen chemical potential gradient dependencies of the steady-state oxygen permeation flux (A) and the corresponding specific oxygen permeability (B) through membranes in the system $Gd_xCe_{0.8-x}Pr_{0.2}O_{2-\delta}$ of $x = 0, 0.15$ and 0.2. Different membrane thicknesses are shown for $x = 0.15$, highlighting surface limitations.

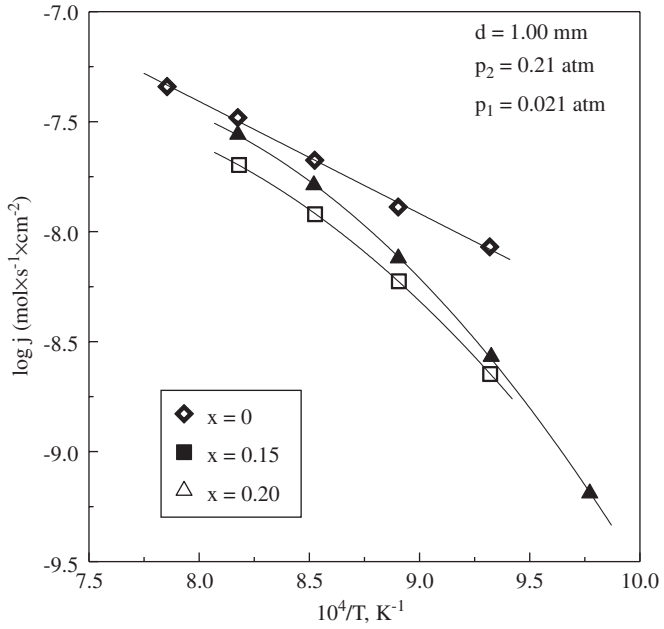

Fig. 8. Comparison of temperature dependence of the oxygen permeation flux in the system $Gd_xCe_{0.8-x}Pr_{0.2}O_{2-\delta}$ for $x = 0, 0.15$ and 0.2, for identical membrane thicknesses and oxygen partial pressure gradients.

Clearly this comparison must be considered only qualitative for two reasons, firstly the pO_2 gradient of the e.m.f. measurements is not the same as the pO_2 gradient in Fig. 8 and secondly the effects of surface exchange are not considered. However, despite these limitations, good agreement is observed between overall trends in ambipolar conductivity and trends in oxygen permeation flux with variations in composition. One can state that the oxygen permeation flux is dominated by the ambipolar conductivity in these materials and the ambipolar conductivity is dominated by the level of electronic conductivity, Fig. 6d. The stronger temperature dependence of the oxygen permeation flux in the Gd-containing materials arises due to the larger activation energy for electronic conduction in these materials, as discussed in the previous section.

4. Conclusions

The extremely high TEC at intermediate temperatures observed in $Ce_{1-y}Pr_yO_{2-\delta}$ materials can be substantially decreased by the substitution of 20 at% Gd for cerium. Materials offering TECs varying between 10 and $18 \times 10^{-6}\,K^{-1}$ across different temperature ranges between

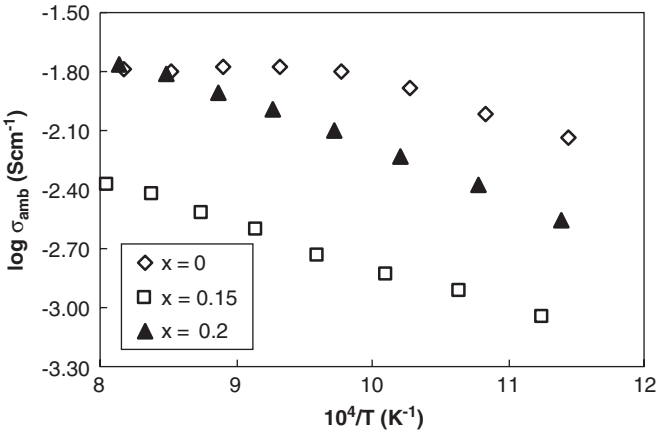

Fig. 9. Temperature dependence of ambipolar conductivities in the system $Gd_xCe_{0.8-x}Pr_{0.2}O_{2-\delta}$ for $x = 0, 0.15$ and 0.2, calculated from results of e.m.f. measurements, Fig. 6a–d.

30 and 1000 °C can be formed. The large increase in thermal expansion rate at intermediate temperatures has its basis in the loss of oxygen upon heating, and the extent of this oxygen exchange is reduced by Gd substitution. Increasing Gd content decreases total, ionic and electronic conductivities, whist grain size is unaffected. Coulometric titration shows that, at elevated temperatures, the average oxidation state of Pr in composition $x = 0.15$ is significantly lower than that found in $x = 0$ or $x = 0.2$, which are shown to be similar. This suggests that the charge compensation mechanism changes with increasing x. In $x = 0.15$, charge compensation is by vacancy formation and destabilises the presence of Pr^{4+}. At $x = 0.2$, further Gd substitution is instead charge compensated by additionally raising the oxidation state of Pr rather than solely the creation of additional oxygen ion vacancies. This can be discussed in terms of increasing defect association with increasing x. This postulated ordering phenomenon would be worth studying further by selected area electron diffraction and high-resolution transmission electron microscopy as successfully performed on other defect fluorite materials [32]. The oxygen permeation fluxes through dense $Gd_xCe_{0.8-x}Pr_{0.2}O_{2-\delta}$ ceramics are limited by both bulk ambipolar conductivity and surface exchange. However, the composition-dependent trends in permeability are shown to be dominated by the level of ambipolar conductivity, and the ambipolar conductivity is dominated by the level of electronic conductivity. At the highest temperatures, oxygen permeability of composition $x = 0.2$ approaches that of composition $x = 0$, $Ce_{0.8}Pr_{0.2}O_{2-\delta}$, but clearly offers much better thermal expansion properties.

Acknowledgments

This work was supported by the FCT, Portugal (projects POCTI/CTM/3938/2001, SFRH/BPD/3529/2000 and SFRH/BD/6595/2001) and the NATO Science for Peace program (project 978002).

Appendix A. Supplementary data

Supplementary data associated with this article can be found in the online version at doi:10.1016/j.jssc.2006.06.028.

References

[1] A.D. Logan, M. Shelef, J. Mater. Res. 9 (1994) 468.
[2] M.Y. Sinev, G.W. Graham, L.P. Haack, M. Shelef, J. Mater. Res. 11 (1996) 1960.
[3] P. Knauth, H.L. Tuller, J. Eur. Ceram. Soc. 19 (1999) 831.
[4] M. Rajendran, K.K. Mallick, A.K. Bhattacharya, J. Mater. Sci. 33 (1998) 5001.
[5] T.S. Stefanik, H.L. Tuller, J. Eur. Ceram. Soc. 21 (2001) 1967.
[6] C.K. Narula, L.P. Haack, W. Chun, H.W. Jen, G.W. Graham, J. Phys. Chem. B 103 (1999) 3634.
[7] S. Rossignol, C. Descorme, C. Kappenstein, D. Duprez, J. Mater. Chem. 11 (2001) 2587.
[8] P. Shuk, M. Greenblatt, Solid State Ionics 116 (1999) 217.
[9] D.P. Fagg, V.V. Kharton, A.L. Shaula, I.P. Marozau, J.R. Frade, Solid State Ionics 176 (2005) 1723.
[10] D.P. Fagg, J.R. Frade, V.V. Kharton, I.P. Marozau, J. Solid State Chem. 179 (2006) 1469.
[11] M. Nauer, C. Ftikos, B.C.H. Steele, J. Eur. Ceram. Soc. 14 (1994) 493.
[12] C. Ftikos, M. Nauer, B.C.H. Steele, J. Eur. Ceram. Soc. 12 (1993) 267.
[13] V.V. Kharton, E.N. Naumovich, A.A. Vecher, A.V. Nikolaev, J. Solid State Chem. 120 (1995) 128.
[14] A.V. Kovalevsky, V.V. Kharton, V.N. Tikhonovich, E.N. Naumovich, A.A. Tonoyan, O.P. Reut, L.S. Boginsky, Mater. Sci. Eng. B 52 (1998) 105.
[15] V.V. Kharton, V.N. Tikhnovich, L. Shuangbao, E.N. Naumovich, A.V. Kovalevsky, A.P. Viskup, I.A. Bashmakov, A.A. Yaremchenko, J. Electrochem. Soc. 145 (1998) 1363.
[16] V.P. Gorelov, Elektrokhimiya 24 (1988) 1380 (in Russian).
[17] V.V. Kharton, F.M.B. Marques, Solid State Ionics 140 (2001) 381.
[18] V.V. Kharton, A.P. Viskup, F.M. Figueiredo, E.N. Naumovich, A.A. Yaremchenko, F.M.B. Marques, Electrochim. Acta 46 (2001) 2879.
[19] H. Hayashi, M. Kanoh, C.J. Quan, H. Inaba, S. Wang, M. Dokiya, H. Tagawa, Solid State Ionics 132 (2000) 227.
[20] H.L. Tuller, in: O. Toft Sørensen (Ed.), Non-Stoichiometric Oxides, Academic Press, New York, 1981, p. 271.
[21] S. Wang, H. Inaba, H. Tagawa, M. Dokiya, T. Hashimoto, Solid State Ionics 107 (1998) 73.
[22] D. Schneider, M. Godickemeier, L. Gaukler, J. Electroceram. 1 (1997) 165.
[23] G. Balducci, M.S. Islam, J. Kašpar, P. Fornasiero, M. Graziani, Chem. Mater. 15 (2003) 3781.
[24] D.J.M. Bevan, J. Kordis, J. Inorg. Nucl. Chem. 26 (1964) 1509.
[25] G. Brouwer, Philips Res. Rep. 9 (1954) 366.
[26] M.S. Jenkins, R.P. Turcotte, L. Eyring, in: L. Eyring, M. O'Keeffe (Eds.), The Chemistry of Extended Defects in Non-Metallic Solids, North-Holland Publ., Amsterdam, 1970, p. 36.
[27] O.T. Sørensen, J. Solid State Chem. 18 (1976) 217.
[28] T. Kudo, H. Obayashi, J. Electrochem. Soc. 123 (3) (1976) 451.
[29] L. Minervini, M.O. Zacate, R.W. Grimes, Solid State Ionics 116 (1999) 339.
[30] J.A. Kilner, B.C.H. Steele, in: O. Toft Sørensen (Ed.), Non-Stoichiometric Oxides, Academic Press, New York, 1981, p. 233.
[31] D.P. Fagg, J.T.S. Irvine, J. Solid State Chem. 172 (2) (2003) 277.
[32] J.T.S. Irvine, A.J. Feighery, D.P. Fagg, S. Garcia-Martin, Solid State Ionics 136 (2000) 879.